A 3-D Structural Model of Solid Self-Assembled Chlorophyll *a*/H₂O from Multispin Labeling and MAS NMR 2-D Dipolar Correlation Spectroscopy in High Magnetic Field

Barth J. van Rossum,* Els A. M. Schulten,* Jan Raap,* Hartmut Oschkinat,† and Huub J. M. de Groot*,1

*Leiden Institute of Chemistry, Gorlaeus Laboratories, Leiden University, Einsteinweg P.O. Box 9502, 2300 RA Leiden, The Netherlands;
and †Forschungsinstitut für Molekulare Pharmakologie, Robert-Rössle Strasse 10, D-13125, Berlin, Germany

Magic angle spinning (MAS) NMR with Lee–Goldburg cross-polarization (LG-CP) is used to promote long-range heteronuclear transfer of magnetization and to constrain a structural model for uniformly labeled chlorophyll *a*/H₂O. An effective maximum transfer range d_{max} can be determined experimentally from the detection of a gradually decreasing series of intramolecular correlations with the ^{13}C along the molecular skeleton. To probe intermolecular contacts, d_{max} can be set to ∼4.2 Å by choosing an LG-CP contact time of 2 ms. Long-range ^{1}H–^{13}C correlations are used in conjunction with carbon and proton aggregation shifts to establish the stacking of the chlorophyll *a* (Chl *a*) molecules. First, high-field (14.1 T) 2-D MAS NMR homonuclear (^{13}C–^{13}C) dipolar correlation spectra provide a complete assignment of the carbon chemical shifts. Second, proton chemical shifts are obtained from ^{1}H–^{13}C heteronuclear dipolar correlation spectroscopy in high magnetic field. The shift constraints and long-range ^{1}H–^{13}C intermolecular correlations reveal a 2-D stacking homologous to the molecular arrangement in crystalline solid ethyl-chlorophyllide *a*. A doubling of a small subset of the carbon resonances, in the 7-methyl region of the molecule, provides evidence for two marginally different well-defined molecular environments. Evidence is found for the presence of neutral structural water molecules forming a hydrogen-bonded network to stabilize Chl *a* sheets. In line with the microcrystalline order observed for the rings, the long T_1's, and absence of conformational shifts for the ^{13}C in the phytyl tails, it is proposed that the Chl *a* form a rigid 3-D space-filling structure. Probably the only way this can be realized with the sheets is by forming bilayers with interpenetration of elongated tails. Such a 3-D space-filling organization of the aggregated Chl *a* from MAS NMR would match existing models inferred from electron microscopy and low-resolution X-ray powder diffraction, while a micellar model based on neutron diffraction and antiparallel stacking observed in solution can be discarded. © 2002 Elsevier Science (USA)

Key Words: solid-state NMR; chlorophyll *a*; dipolar correlation spectroscopy, frequency-switched Lee–Goldburg; homology modeling.

INTRODUCTION

It has been demonstrated recently that concepts for MAS NMR structure determination using dipolar correlation spectroscopy and multispin labeling exist (*1*). In a first successful attempt to perform *de novo* structure determination, the homonuclear radiofrequency-driven dipolar recoupling (RFDR) technique was applied to aggregated uniformly ^{13}C-enriched Chl *a* and its structure was partially resolved (*1*). Recently the first application of similar strategies to a synthetic system was reported (*2*). In addition, for small uniformly ^{13}C-labeled molecules in the solid state, well-resolved ^{1}H–^{13}C MAS NMR heteronuclear dipolar correlation spectra can be obtained in high magnetic field with fast MAS using 2-D frequency-switched Lee–Goldburg (FSLG) techniques that are easy to implement (*3, 4*). From the coherent transfer during short Lee–Goldburg Cross-Polarization (LG-CP) mixing times, short-range intermolecular ^{1}H–^{13}C distances for the characterization of hydrogen bond structure can be determined accurately (*5*). It will be shown here how long-range ^{1}H–^{13}C heteronuclear intermolecular correlations can be obtained from weak transfer processes occurring on a longer time scale in the LG-CP. The dipolar correlations are used in conjunction with shifts to establish the stacking of the chlorophyll molecules. In addition, we aim at the specification of how the stacked Chl *a*/H₂O can be organized to yield a space-filled 3-D model that optimally fits all the available MAS NMR data.

Chl *a* is the green pigment involved in photosynthetic harvesting of light and subsequent conversion of light energy into chemical energy by plants and related species, like algae and cyanobacteria (Fig. 1). Chl *a* self-assembles in hexane in the presence of H₂O (*6*). The molecular arrangement of Chl *a*/H₂O is thought to represent a paradigm for a special type of photosynthetic light-harvesting system, the chlorosome antenna found in some photosynthetic bacteria. This antenna system is almost protein-free and is potentially important for artificial photosynthesis research (*7*).

1 To whom correspondence should be addressed. Fax: (+31) 71 527 4603. E-mail: groot_h@chem.leidenuniv.nl.
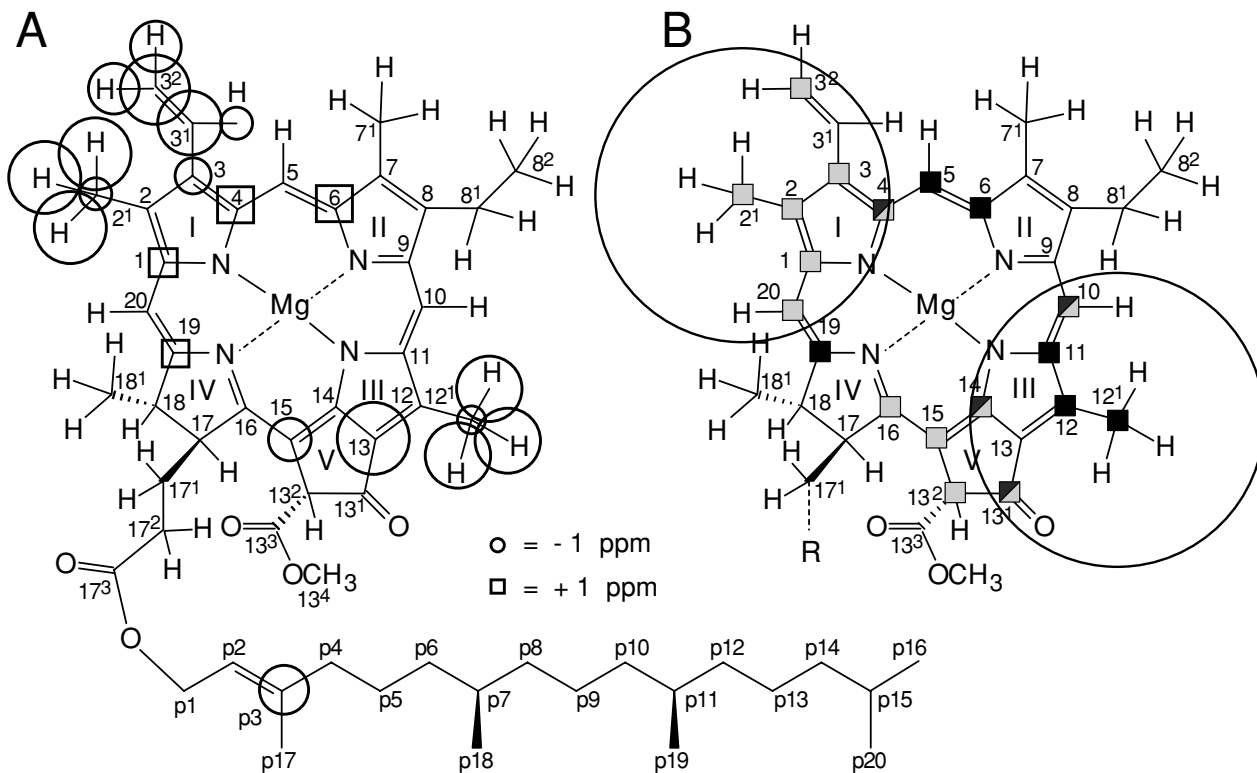
FIG. 1. (A) Visual representation of the carbon and proton aggregation shifts $\Delta\sigma$ for aggregated Chl a. The circles around the carbon and hydrogen atoms represent upfield aggregation shifts; squares represent downfield shifts. The sizes of the circles and squares reflect the magnitude of the aggregation shifts. (B) Schematic representation of the assignment of heteronuclear correlations involving the 2^1-H_3 (shaded gray) or the 12^1-H_3 (solid black). For the 4-C, 10-C, 13^1-C, and 14-C the correlations with proton signals are assigned to transfer from both methyl groups. The ranges for intramolecular transfer for the two methyl groups are indicated with the circles. Intramolecular correlations involving the 3^1-C and 13-C could not be assigned.

RESULTS

To obtain a complete ^{13}C assignment for the Chl a/H$_2$O, homonuclear (^{13}C–^{13}C) dipolar correlation spectra were recorded with MAS rates of 12 or 13 kHz and with different homonuclear mixing times. The resolution in the high-field RFDR spectra is considerably improved compared to earlier work in a lower field (1). The ^{13}C lines are narrow and the widths range from 120 to 200 Hz, due to the J-couplings between the ^{13}C nuclei in the uniformly labeled Chl a. The narrow ^{13}C lines reflect a high sample quality.

An analysis of RFDR correlation spectra obtained from [U-^{13}C]Chl a/H$_2$O aggregates has been reported previously and the discussion here will focus on the refinements that can be obtained in ultrahigh field (1). Due to the improved resolution in the higher field, the 7^1-C and 12^1-C signals that were not yet resolved in previous studies can be assigned unambiguously. Figure 2 shows several sections of a high-field (14.1 T) ^{13}C RFDR homonuclear dipolar correlation spectrum recorded with a mixing time of 2.46 ms and using a spinning frequency $\omega_r/2\pi = 13$ kHz. The correlation networks displayed in Fig. 2A connect the 10-11-12-12^1-13 (solid lines), 4-5-6-7-7^1-8 (dashed lines), and 20-1-2-2^1-3 (dot-dashed lines), and confirm the as-

signment of the 7^1-C and 12^1-C resonances. The correlations of the 7-C with the 6-C and 8-C reveal a small but resolved doubling of the 7-C response, with the two resonances separated by 1.1 ppm. In addition, a separation corresponding with 2.6 ppm is observed for the 7^1-C response. This signal doubling is shown in detail in Figs. 2B and 2C. Three cross peaks that can be assigned to correlations of the 8^1-C or 8^2-C with the 8-C are observed (Fig. 2C). Since two weak correlations appear for the 8^1-C with the 7-C, at least the signal from the 8^1-C is doubled, while the data suggest an additional doubling of the 8^2-C. The refined ^{13}C assignment is listed in Table 1. For the correlations that are doubled and resolved in the homonuclear correlation spectrum, the relative intensities of the two components can be estimated from the integrated peak volumes: $7^1(11.5)/8 : 7^1(8.9)/8 = 47 : 53; 7^1(11.5)/6 : 7^1(8.9)/6 = 56 : 44$, and $7(132.2)/6 : 7(133.3)/6 = 50 : 50$, and $8/7(132.2) : 8/7(133.3) = 40 : 60$.

Following the complete ^{13}C assignment, individual proton resonances can be assigned and intermolecular distance constraints can be determined with FSLG heteronuclear dipolar correlation spectroscopy (Fig. 3) (8). During the LG-CP, an off-resonance RF field locks the proton spins in the rotating frame along an axis inclined at the magic angle with respect to the static field in the z-direction, while the carbon spins are locked
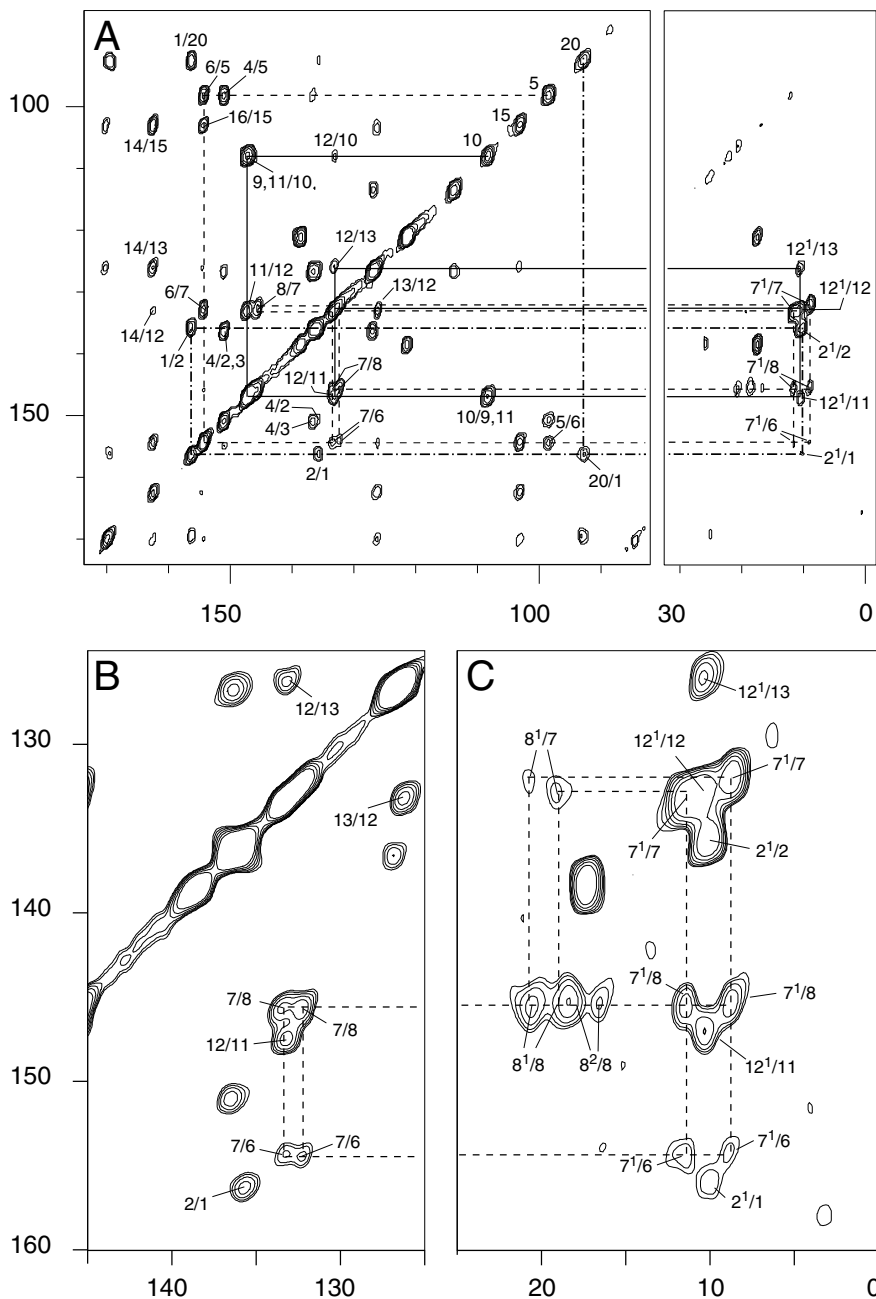
FIG. 2. Contour plots of a 2-D MAS NMR homonuclear (^{13}C–^{13}C) dipolar correlation spectrum of uniformly ^{13}C-enriched Chl *a*/H_2O aggregates, recorded in a magnetic field of 14.1 T with a spinning rate of 13 kHz and using a homonuclear polarization transfer time of 2.46 ms. In (A), the correlation networks are shown that are relevant for the assignment of the 2^1, 7^1, and 12^1 signals. Solid lines connect the 10-11-12-12^1-13, dashed lines the 4-5-6-7-7^1-8, and dot-dashed lines the 20-1-2-2^1-3. The doubling of the 7-C is illustrated in detail in (B); the doublings of the 7^1-C and 8^1-C are illustrated in (C). For clarity, only the correlation network involving the 6-7-7^1-8-8^1-8^2 is drawn in (B) and (C). The numbering in the plots corresponds to the numbering in Fig. 1.

on-resonance in the *xy*-plane. In this way, heteronuclear spin locking with simultaneous suppression of the homonuclear dipolar proton coupling is achieved and polarization can be transferred selectively from the protons to the carbon nuclei (*5*).

For the ^1H assignments we have recorded data with a short CP contact time of 600 μs to build up short-range heteronuclear correlations. Due to the high resolution in the carbon dimen-

sion, it is possible to assign nearly all Chl *a* ^1H resonances from 2-D heteronuclear dipolar correlation spectroscopy (Table 1). The solid-state assignments of the 17-H and 13^4-H_3 responses are tentative due to spectral overlap in the ^{13}C dimension. The assignment of the 8^1-CH_2 is difficult because of overlap of the correlations with the strong signals from the P7-Me and P11-Me moieties. Using the assignments listed in Tables 1 and 2

TABLE 1
^{13}C and ^{1}H Chemical Shifts and Aggregation Shifts for Chl a/H$_2$O

Position	σ^C (ppm)	$\Delta\sigma^C$ (ppm)	σ^H (ppm)	$\Delta\sigma^H$ (ppm)
12[1]	10.5 (0.3)	−2.1	−1.3 (0.3)	−4.9
2[1]	10.2 (0.2)	−2.4	−2.1 (0.3)	−5.4
7[1]	8.9/11.5 (0.2)	−2.3/0.3	1.7/2.8 (0.3)	−1.6/−0.5
P17	17.4 (0.1)	1.2	1.5 (0.5)	0.0
8[2]	16.5/17.5 (0.5)	−1.5/−0.5	1(1)	−0.7
8[1]	19.0/20.5 (0.5)	−1.0/0.5	2(2)	−2
P18	20.0 (0.2)	0.0	0.9 (0.5)	0.1
P19	20.0 (0.2)	0.0	0.9 (0.5)	0.1
P20	23.3 (0.3)	0.3	1 (1)	0.2
P16	23.3 (0.3)	0.3	1 (1)	0.2
18[1]	24.9 (0.1)	1.0	1.4 (0.5)	−0.4
P9	25.6 (0.3)	0.4	1.2 (0.5)	0.0
P13	25.6 (0.3)	0.0	1.2 (0.5)	0.0
P5	25.8 (0.2)	0.0	1.2 (0.5)	0.0
P15	28.4 (0.2)	−0.3	1.3 (0.5)	−0.2
17[1]	32.3 (0.1)	2.2/1.3[a]	3.0 (0.5)	0.5
17[2]	32.3 (0.1)	2.2/1.3[a]	3.0 (0.5)	1.0
P7	33.1 (0.1)	−0.3	1.2 (0.5)	−0.1
P11	33.1 (0.1)	−0.5	1.2 (0.5)	−0.1
P6	37.1 (0.5)	−0.3	1.0 (0.5)	−0.1
P12	38.0 (0.2)	0.0	1.1 (0.5)	0.0
P8	38.0 (0.2)	0.0	1.1 (0.5)	0.0
P10	38.0 (0.2)	0.0	1.1 (0.5)	0.0
P14	40.0 (0.2)	−0.1	2.0 (0.5)	0.9
P4	40.0 (0.2)	−0.4	2.0 (0.5)	0.2
18	50.0 (0.1)	0.0	2.8 (0.5)	−1.8
17	51.7 (0.3)	0.1	3.9 (0.5)	−0.3
13[4]	51.8 (0.1)	−0.2	3.4 (0.5)	−0.4
P1	61.7 (0.1)	0.4	4.9 (0.3)	0.6
13[2]	64.9 (0.1)	−1.3	5.8 (0.5)	−0.4
20	92.6 (0.2)	−0.2	6.7 (0.3)	−1.9
5	98.3 (0.1)	−1.7	8.6 (0.3)	−0.8
15	103.0 (0.1)	−3.2		
10	108.1 (0.1)	1.0	7.8 (0.3)	−1.9
3[2]	113.7 (0.1)	−5.2	2.3 (0.5)	−3.9/−3.7
P2	121.3 (0.1)	1.9	6.0 (0.3)	1.0
13	126.1 (0.1)	−5.4		
3[1]	126.7 (0.1)	−4.8	5.7 (0.3)	−2.4
7	132.2/133.3 (0.1)	−1.8/−0.7		
12	133.0 (0.1)	−1.2		
2	135.6 (0.1)	0.1		
3	136.3 (0.1)	−2.7		
P3	138.5 (0.1)	−3.7		
8	145.4 (0.1)	1.3		
9/11	147.0 (0.1)	0.9/−0.7[a]		
4	150.7 (0.1)	2.7		
6	154.1 (0.2)	2.7		
16	154.0 (0.1)	−1.8		
1	156.1 (0.1)	2.1		
14	162.3 (0.1)	0.9		
19	169.4 (0.3)	2.0		
13[3]	169.9 (0.1)	−1.1		
17[3]	174.3 (0.3)	1.6		
13[1]	190.6 (0.1)	1.3		

Note. The estimated errors for the solid-state shifts are given in parentheses. The numbering is according to Fig. 1.

[a] The differences between 9-C/11-C and between 17^1-C/17^2-C are not resolved in solution.

TABLE 2
Chemical Shifts (σ^C_{liq}, σ^H_{liq}), for Monomeric Chl a in Acetone-d_6, Used for the Calculation of the $\Delta\sigma$

Position	σ^C_{liq} (ppm)	σ^H_{liq} (ppm)
12[1]	12.6	3.60
2[1]	12.6	3.34
7[1]	11.2	3.29
P17	16.2	1.52
8[2]	18.0	1.70
8[1]	20.0	3.79
P18	20.0	0.80
P19	20.0	0.80
P20	23.0	0.85
P16	23.0	0.85
18[1]	23.9	1.77
P9	25.2	1.2
P13	25.6	1.2
P5	25.8	1.2
P15	28.7	1.51
17[1] [a]	30.1/30.9	2.63–2.54/2.49–2.38
17[2] [a]	30.1/30.9	2.05
P7	33.4	1.33
P11	33.6	1.33
P6	37.4	1.2–1.0
P12	38.0	1.2–1.0
P8	38.0	1.2–1.0
P10	38.0	1.2–1.0
P14	40.1	1.12
P4	40.4	1.82
18	50.0	4.56
17	51.6	4.18
13[4]	52.0	3.82
P1	61.3	4.36/4.26
13[2]	66.2	6.20
20	92.8	8.56
5	100.0	9.40
15	106.2	
10	107.1	9.72
3[2]	118.9	6.22/6.01
P2	119.4	5.01
13	131.5	
3[1]	131.5	8.12
7	134.0	
12	134.2	
2	135.5	
3	139.0	
P3	142.2	
8	144.1	
9/11[a]	146.1/147.7	
4	148.0	
6	151.4	
16	155.8	
1	154.0	
14	161.4	
19	167.4	
13[3]	171.0	
17[3]	172.7	
13[1]	189.3	

Note. Compiled information from this work and published sources (*23, 30, 31*). The numbering is according to Fig. 1.

[a] Not fully resolved.
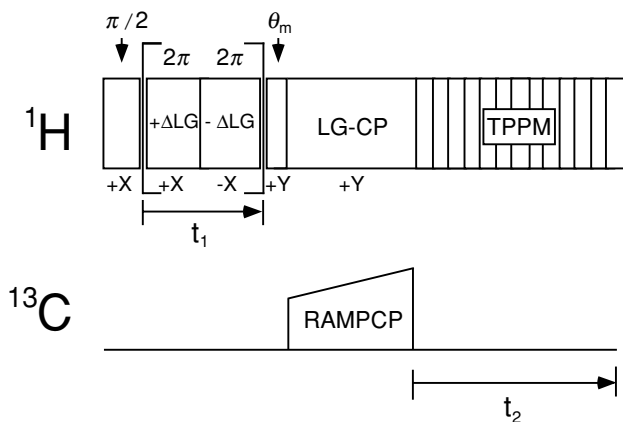
FIG. 3. Pulse program for FSLG ^{1}H homonuclear-decoupled heteronuclear (^{1}H–^{13}C) dipolar correlation spectroscopy.

for the shifts σ in the solid state and σ_{liq} in solution, respectively, aggregation shifts $\Delta\sigma = \sigma - \sigma_{\text{liq}}$ were calculated, and the $|\Delta\sigma| > 2$ ppm are visualized in Fig. 1A. The $\Delta\sigma$ reflect the differences in the molecular electronic structure between the monomeric and the aggregated form. The larger proton aggregation shifts $|\Delta\sigma^H| > 2$ ppm are all upfield and are detected for the side-chain hydrogens 2^1-H$_3$ (−5.4 ppm), 3^1-H (−2.4 ppm), 3^2-H$_2$ (−3.8 ppm), and 12^1-H$_3$ (−4.9 ppm).

It has been demonstrated recently that even in its most simple form, high-field heteronuclear correlation spectroscopy provides access to intermolecular correlations (*9*). There are several advantages in using ^{1}H–^{13}C heteronuclear dipolar correlation spectroscopy instead of homonuclear ^{13}C methods for collecting long-range intermolecular constraints. First, the gyromagnetic ratio for protons is four times larger than that for carbon nuclei. Second, the heteronuclear spin topology of hydrocarbons favors the detection of intermolecular ^{1}H–^{13}C correlations, since protons are generally located at the exterior of the molecule and are often in contact with carbons. Finally, a distinction between relayed intramolecular and intermolecular homonuclear ^{13}C coherence transfer is difficult due to rapid spin diffusion in multispin ^{13}C networks, while for heteronuclear correlation spectroscopy spin diffusion among protons can be suppressed effectively by the application of ^{1}H homonuclear decoupling sequences during the transfer period.

Intermolecular heteronuclear correlations involve transfer of magnetization over relatively long distances, ~4 Å. This corresponds with a heteronuclear dipolar coupling of ~200 Hz and requires a relatively long transfer time. The ^{1}H resolution and selectivity of the ^{1}H–^{13}C transfer can be optimized effectively by applying high-field, fast spinning, and LG decoupling sequences during ^{1}H evolution and cross-polarization (*4, 5*). It has been shown that protons in NH$_3$ or CH$_3$ groups can transfer magnetization over considerable distances (*4, 8*). This provides an attractive route to the detection of intermolecular transfer events. It contrasts with the rapid coherent transfer with a dephasing time of ~1 ms during LG-CP of a proton that is directly bonded to a ^{13}C or protons in hydrogen bonds (*5*).

The long-range correlations can provide distance restraints and structural information. Figure 4 shows a high-field heteronuclear correlation spectrum recorded with a MAS rate $\omega_r/2\pi = 13$ kHz using the pulse sequence of Fig. 3, with ^{1}H homonuclear FSLG decoupling during proton evolution (*4*). A
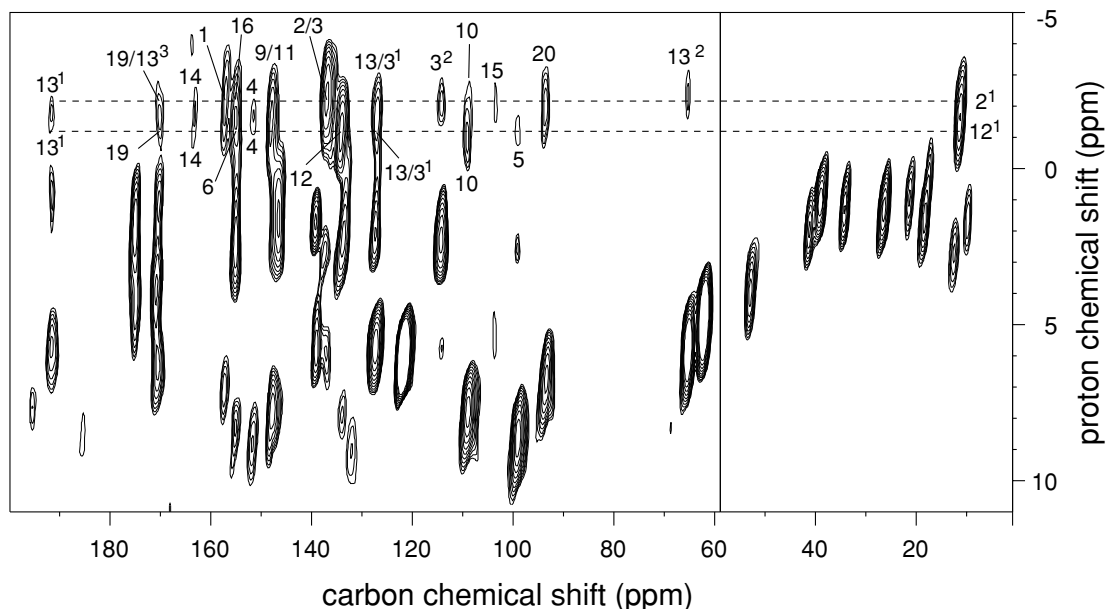
FIG. 4. Contour plot of a 2-D MAS NMR heteronuclear (^{1}H–^{13}C) FSLG-decoupled dipolar correlation spectrum recorded from uniformly ^{13}C-enriched Chl *a*/H$_2$O aggregates. The data were collected in a field of 14.1 T and with a spinning speed of 13 kHz. A LG-CP contact time of 2 ms was applied. The lines indicate the proton shifts for the 2^1-H$_3$ (upper trace) and for the 12^1-H$_3$ (lower trace). The numbering in the plot corresponds to the numbering in Fig. 1.

long LG-CP mixing period of 2 ms was applied to promote proton polarization transfer that reveals the spatial arrangement of the molecules in the solid. Many correlations involving the 2^1-H_3 and 12^1-H_3 are well resolved due to the pronounced upfield ring-current shifts of the 2^1 and 12^1 methyl protons (Fig. 4). The 2^1-H_3 resonate with $\sigma^H = -2.1$ ppm and can be unambiguously assigned from strong correlations with the nearby 2-C and 3-C, in the aromatic region of the ^{13}C dimension. The intensity of these signals is ~25% of the signal strength of the correlation with the directly bonded 2^1-C. The 12^1-H_3 resonate with $\sigma^H = -1.3$ ppm and are assigned from the strong correlation with the 12-C. The dashed horizontal lines in Fig. 4 mark the ^{1}H shifts of the protons in the two methyl groups. They are of assistance in assigning the remaining heteronuclear correlation signals that fall into three categories: (i) resolved, (ii) less resolved in ^{1}H, resolved in ^{13}C, and (iii) less resolved in both the ^{1}H and the ^{13}C dimensions.

(i) In the first category, the 2^1-H_3 have resolved intramolecular correlations with the 1-, 2-, 3-, 3^2-, and 20-C. This set of intarmolecular correlations reveals an effective range $d_{max} \sim 4.2$ Å for the detection of heteronuclear signals, since the intramolecular correlation between the 2^1-H_3 and the 4-C over ~4.2 Å is very weak and there is no evidence for an intramolecular correlation signal between the 2^1-H_3 and the 5-C, over a distance of ~5.5 Å. This illustrates the selectivity of the experiment of Fig. 3 with respect to the detection range d_{max}. The dipolar interaction decreases rapidly with the third power of the internuclear distance and this effectively suppresses longer range transfers.

Two additional resolved correlation signals are observed for the 2^1-H_3 with the 13^2-C and 15-C at the opposite side of the Chl a molecule, clearly outside the range for intramolecular transfer events. These signals are weak and are attributed to intermolecular heteronuclear polarization transfer. They show that magnetization can be transferred during LG-CP from the methyl side chains to carbons in the ring of a nearby Chl a molecule. In a similar manner, the 12^1-H_3 yield resolved intramolecular correlations with the nearby 10-C and 12-C, while a weak intermolecular correlation with the 5-C is also resolved. Since the shortest possible distance for intermolecular transfer will be approximately 4 Å, the detection of weak intermolecular transfer events proves that the d_{max} is not overestimated, due to, e.g., enhanced polarization transfer by intramolecular spin diffusion type processes during the LG-CP.

(ii) Several cross peaks are not completely resolved due to the partial overlap of the responses from both methyl groups in the ^{1}H dimension. The most prominent examples in this category are obviously the very intense one-bond correlation signals of the 2^1-H_3 with the 2^1-C and of the 12^1-H_3 with the 12^1-C, which give rise to a single broad peak in the ^{1}H dimension in between the two dashed lines in Fig. 4 with $\sigma^C \sim 10.3$ ppm. A qualitatively similar response in the ^{1}H dimension is observed for the correlations with the 4-C, the 14-C, and the 13^1-C. These weak signals are well resolved in the ^{13}C dimension and are attributed to long-range transfer events from the 2^1-H_3 and the 12^1-H_3 to the same type of ^{13}C. Considering $d_{max} \sim 4.2$ Å, the correlations of the 2^1-H_3 with 13^1-C or 14-C and of the 12^1-H_3 with 4-C should be identified with intermolecular transfer. In addition, the resolved moderately strong intramolecular correlation of the 12^1-H_3 with the 10-C with $\sigma^C = 108.1$ ppm comprises an upfield shoulder with $\sigma^H = -2.1$ ppm, which is attributed to weak intermolecular transfer between the 2^1-H_3 moiety and a 10-C of a nearby molecule.

(iii) A number of correlation signals are neither fully resolved in the ^{1}H nor in the ^{13}C dimension. The designation of these signals should be consistent with the partial assignment obtained thus far and with general constraints set by the detection range. For instance, a moderately strong correlation signal with $\sigma^C = 154$ ppm and σ^H in between the dashed lines is observed in the data presented in Fig. 4. This relatively weak signal is superimposed on a strong background signal involving the 6-C or the 16-C. This signal will be attributed to intermolecular transfer from the 2^1-H_3 to the 16-C and from the 12^1-H_3 to the 6-C, in line with the observation of intermolecular transfer from the 2^1-H_3 to the 15-C and from the 12^1-H_3 to the 5-C in category (i). A contribution from intramolecular transfer is unlikely. The shortest intramolecular distances are ~6.5 Å, from the 2^1-H_3 to the 6-C and from the 12^1-H_3 to the 16-C. This is well beyond the d_{max} obtained from the intramolecular correlations. Intermolecular transfer from the 2^1-H_3 to the 6-C or from the 12^1-H_3 to the 16-C is also unlikely, since there are no correlation signals with the adjacent carbons, e.g., from the 2^1-H_3 to the 5-C or from the 12^1-H_3 to the 15-C.

Next, a weak correlation signal with $\sigma^C \sim 169.7$ ppm is probably due to transfer involving both the 19-C and the 13^3-C, which resonate with $\sigma^C \sim 169.4$ and $\sigma^C \sim 169.9$ ppm, respectively. They correlate weakly with overlapping proton signals with an average $\sigma^H \sim -1.7$ ppm in between the dashed lines in Fig. 4. This correlation signal is attributed to magnetization transfer from 2^1-H_3 to 19-C and/or 13^3-C with $\sigma^H = -2.1$ ppm, overlapping with an intermolecular transfer signal from 12^1-H_3 to 19-C with $\sigma^H = -1.3$ ppm. An intramolecular correlation between 2^1-H_3 and 19-C is a possibility, since the distance is ~4 Å, close to the limit of the transfer range. In parallel, intermolecular transfer from 2^1-H_3 to 13^3-C would be in line with the observation of the fully resolved correlation between the 2^1-H_3 and the 13^2-C in the first category. In contrast, the distance between the 12^1-H_3 and the 13^3-C is ~6 Å. This is well beyond d_{max} and intramolecular transfer between the 12^1-H_3 and the 13^3-C during the LG-CP time of 2 ms is very unlikely. Therefore the contribution from the 12^1-H_3 is attributed to intermolecular transfer to the 19-C.

Two correlation signals are difficult to assign. The first is a correlation involving the 9-C and 11-C. The major part of this signal is probably due to intramolecular transfer from the 12^1-H_3 to the 11-C, which is well within range, at a distance of 2.8 Å $< d_{max}$.

In addition there is a shoulder revealing weak transfer from the 2^1-H$_3$. At this stage an unambiguous assignment of this feature is not possible. Most likely the transfer is to the 9-C, in line with the structural model presented in the next section. Finally there is a correlation with $\sigma^C \sim 126.4$ ppm. This correlation is most likely in part due to intramolecular transfer events, from the 2^1-H$_3$ to the 3^1-C and from the 12^1-H$_3$ to the 13-C. In addition, weak intermolecular transfer, from the 2^1-H$_3$ to the 13-C and from the 12^1-H$_3$ to the 3^1-C, would be consistent with the global pattern of heteronuclear correlations depicted in Fig. 1B.

The detection of long-range transfer involving the 2^1-H$_3$ and the 12^1-H$_3$ is possible since they are upfield shifted. In contrast, due to the considerable spectral overlap of the ^{1}H response we have not been able to detect long-range intermolecular correlations between protons on the rings or between protons on the tails.

DISCUSSION

MAS dipolar recoupling sequences were initially used in moderately high field to confirm and refine structures by selective measurement of distances between pairs of labels in specially prepared samples (*10–13*). In this study MAS NMR dipolar recoupling techniques are applied to obtain carbon and proton assignments, aggregation shifts, and long-range ^{1}H–^{13}C correlations. According to NMR, Chl a/H$_2$O is microscopically ordered and the molecules constituting the aggregate are tightly held in place. A structural model for the stacking in this aggregate can be established in steps. It suggests a bilayer space-filling organization for the self-assembled aggregate.

The $\Delta\sigma$ in Table 1 can be used to assess the variations of the atomic charge densities induced by the aggregation process. In a first-order approximation, 1 electronic equivalent of atomic charge difference corresponds with 150 ppm shift difference (*14*). Semiempirical quantum chemical calculations have often been used successfully to translate electronic structure differences for individual atoms into a self-consistent picture on a molecular level (*15, 16*). In model calculations for two different structures, with either H$_2$O or THF coordinating the Mg, the atomic charge density differences for the macrocycle 1-C–20-C are the same within 0.01 electronic equivalent (*17*). This supports conclusions from earlier work on these aggregates that the diamagnetic susceptibility changes observed with NMR through $\Delta\sigma$ are indeed associated with intermolecular stacking effects in the self-assembled Chl a (*1*).

The $\Delta\sigma^H$ provide additional support for the molecular overlap model that was derived from shift and distance constraints obtained with ^{13}C homonuclear dipolar correlation spectroscopy (*1*). The NMR resonances of the 2^1-CH$_3$, 3^1-CH, and 3^2-CH$_2$ moieties at one side of the molecule and of the 12^1-CH$_3$, 13-C, and 15-C moieties at the opposite side are shifted upfield with respect to the corresponding responses for the monomer in solution (Fig. 1A). The pattern of proton aggregation shifts in Fig. 1A confirms that opposite regions, around rings I and III/V, of the Chl a macroaromatic cycle are predominantly affected upon aggregation. This strongly indicates an arrangement of Chl a in linear stacks, with ring I of one molecule placed over rings III and V of a neighboring molecule (Fig. 5, top panel), since substantial ring-current shifts are expected for protons that reside above the ring of adjacent Chl a molecules (*18*).

In addition, the positive $\Delta\sigma^C$ detected for the 19-, 1-, 4-, and 6-C positions indicate the stabilization of a small amount of positive charge in the macroaromatic cycle at both sides of ring I. Although the net charge involved represents only a few percent of an electronic charge equivalent, the pattern of the polarization, odd-numbered carbons at one side of ring I and even-numbered carbons at the other side of ring I, reflects the characteristic bipolaronic pattern of a charge density polarization by an external charge or dipole on an aromatic or olefinic system (*19*). One of the partial negative charges in the system, the 13^1 keto carbonyl oxygen of a chlorophyll neighbor in the assembly, is located about 3.5 Å above the ring I nitrogen and the 1-C and 20-C in the parallel overlap arrangement. Mutual polarization effects involving the 13^1 in this position will contribute to the observed red shift of the Q_y transition and to the stabilization of the aggregate. This shift in the optical spectrum produced by the aggregation is well documented in the literature and a discussion of it is outside the scope of this paper (*20*).

One step forward in this study is the detection of heteronuclear intermolecular correlations in Fig. 4 that firmly establish a parallel stacking. Several correlation signals are associated with the intermolecular transfer of polarization within the stacks. The integrated intensities of intermolecular correlations in Fig. 4 are of the same order of magnitude as the longest range intramolecular correlations. This implies that the intermolecular distances are approximately equal to d_{max}, since the buildup rate of a cross peak depends strongly on the heteronuclear distance. Hence, the sets of intermolecular correlations of the 2^1-H$_3$ with 14-, 15-, 16-, and 13^2-C, and of the 12^1-H$_3$ with the 4-, 5-, and 6-C, provide strong evidence that both methyl groups are $\sim$4 Å above the plane of a neighboring molecule (Fig. 5, top). The weak correlations, from the 2^1-H$_3$ to the 10-C and from the 12^1-H$_3$ to the 19-C, are attributed to intermolecular transfer in the direction perpendicular to the linear stack (Fig. 5, bottom). They confirm the 2-D arrangement of the chlorophyll. They are in line with the excess ring-current shifts $\Delta\sigma^H = -5.4$ ppm and $\Delta\sigma^H = -4.9$ ppm for the 2^1-H$_3$ and the 12^1-H$_3$ (*vide infra*), and homonuclear correlation studies (*1*).

Chl a can form dimers in solution and it has been proposed that dimer structures can possibly serve as a building block for the solid aggregate (*21*). For all dimer models from the solution studies the mutual orientation of the Chl a molecules is antiparallel with ring IV of one molecule positioned above rings III and V of another molecule. This contrasts with the distance information and the pattern of shifts observed for Chl a in the solid aggregate. The largest $\Delta\sigma$ in the dimer building block are consistently observed in the regions around rings IV and III/V
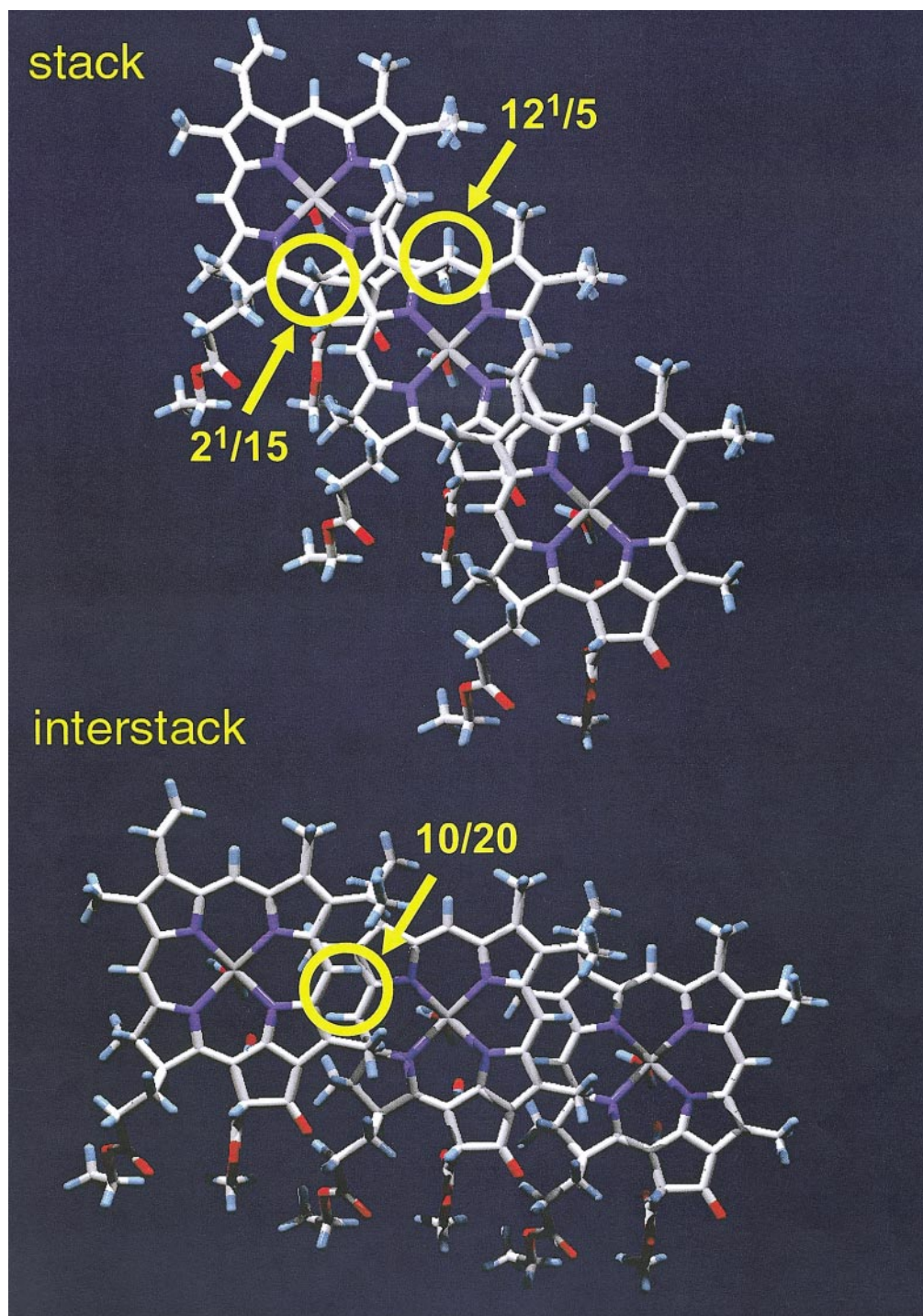
FIG. 5. The overlap with adjacent molecules for the 2^1 and the 12^1 is illustrated with an overlap diagram for molecules within the stack (top) and between stacks (bottom) for the structure of the aggregate according to MAS NMR, which appears in many details homologous to the structure of the ethyl-chlorophyllide *a* from Ref. (*24*). The circles indicate the observed intermolecular ring contacts $2^1/15$ and $12^1/5$ (top) and 10/20 (bottom). The orientation of the chlorophyllide rings is in line with Fig. 1.

(*21–23*). In contrast, the pattern of shifts observed for Chl *a* in the solid aggregate predominantly involves the side chains of ring I. The possibility of an antiparallel dimer building block for the aggregate structure is thus rejected. It was inferred from small-angle neutron scattering that hydrated Chl *a* forms monolayers in a nonpolar solvent that organize into tubular micelles with a fixed radius of ~57 Å, with the phytyl chains on the outside, and with solvent molecules in the interior (*6, 20*). Such a tube filled with solvent is very difficult to reconcile with the NMR data, since a response of the *n*-heptane was not yet observed in any of the datasets. In the sample used for our NMR experiments essentially all the solvent was evaporated and the very narrow NMR lines provide strong evidence for a highly microcrystalline ordered space-filled structure, despite an amorphous appearance in the X-ray diffraction (data not shown).

In contrast with the studies for oligomers in solution and neutron diffraction studies, our MAS shift constraints and heteronuclear intermolecular correlations reveal a close structural homology between the Chl *a* aggregate and an earlier model, based on crystalline ethyl-chlorophyllide *a*/H$_2$O, i.e., the molecule without the phytyl tail (*24*). According to the crystal structure of this analogue there are intermolecular contacts involving methyl protons and aromatic ring carbons that match precisely our distance constraints. The average CH distances d in the overlap regions in the MAS NMR structural model of the Chl *a* stack in Fig. 5 correspond with the shortest heteronuclear intermolecular distances in the X-ray structure of the solid analogue. According to the X-ray structure, these distances are between 3.7 and 4.1 Å, for the 2^1-H$_3$ with the region centered around the 15-C of another molecule and for the 12^1-H$_3$ with the area around the 5-C of a neighbor (*24*).

In the model of Fig. 5, the intrastack and interstack overlap regions that affect the methyl groups are shown. In the stack, the 12-Me protons are located at an average distance of ~3.7 Å above the 5-C of an adjacent Chl *a*. According to calculations for the ring-current effects at various distances above a porphyrin plane (*18*), an upfield shift between −2.0 ppm (4.0 Å above the plane) and −2.5 ppm (3.5 Å) is estimated. Likewise, the 2-Me are at an average distance of 3.8 Å above the 15-C of a next Chl *a* in the stack, leading to a slightly smaller estimate for the shift of approximately −2 ppm. Due to overlap between stacks, the 12-Me protons are also at an average distance of 3.7 Å above the plane of a Chl *a* in a neighboring stack, in between the 20-C and the nitrogen of ring IV. For this positioning we estimate an upfield shift between −2.5 ppm (4.0 Å) and −3.0 ppm (3.5 Å). The 2-Me protons are positioned at a distance of 3.7 Å between the 10-C and the N of ring II, but closer to the Mg than the 12-Me protons, leading to an estimate of −3.0 ppm (4.0 Å) to −3.5 ppm (3.5 Å) for the ring-current shift from the interstack overlap. The total of −4 to −6 ppm compares well with the experimentally observed $\Delta\sigma^H = -5.4$ ppm and $\Delta\sigma^H = -4.9$ ppm for the 2^1-H$_3$ and the 12^1-H$_3$, respectively. Hence, the $\Delta\sigma^H$ for the 2^1-H$_3$ and 12^1-H$_3$ can be quantitatively

understood by taking into account additional ring-current shifts from interstack overlap in the model of Fig. 5. In addition, the 10-H and 20-H are above the plane of the conjugated ring of a Chl *a* molecule in the adjacent stacks. The 10-H is at a distance $d = 3.5$ Å from the 2-C, while the 20-H is at a distance $d = 3.9$ Å from the 11-C and 12-C of another molecule. Upfield proton aggregation shifts of −1.5 to −2.0 ppm can be expected for both the 10-H and the 20-H due to the interstack overlap. This is also well in line with the $\Delta\sigma^H = -1.9$ ppm observed experimentally (Table 1). The NMR data thus provide converging evidence for a structural homology on the atomic level between the Chl *a* aggregate and solid ethyl-chlorophyllide *a*/H$_2$O.

During the preparation of the aggregate water is added. The 2-D ^{1}H–^{13}C spectrum in Fig. 4 reveals weak ^{1}H–^{13}C correlations at the 13^1, 13^3, and 17^3 carbonyl ^{13}C frequencies that are not associated with chlorophyll protons. The 13^1-C=O with $\sigma^C = 190.6$ ppm weakly correlates with overlapping proton signals with $\sigma^H \sim 0.9$ ppm and $\sigma^H \sim -1.7$ ppm. The intensity with $\sigma^H \sim -1.7$ ppm is attributed to intramolecular transfer from the 12^1-H$_3$ and intermolecular transfer from the 2^1-H$_3$, while the signal at 0.9 ppm was not yet assigned. The 17^3-C=O response with $\sigma^C = 174.3$ ppm comprises a broad correlation signal with $\sigma^H \sim 1.7$ ppm that is difficult to reconcile with transfer from the 12^1-H$_3$ or the 2^1-H$_3$, while the 13^3-C=O with $\sigma^C \sim 170$ ppm has a correlation with $\sigma^H = 1.0$ ppm that is unaccounted for. We attribute the signals that remain after the assignment of the Chl *a* proton response and the intermolecular correlations to the NMR of structural water molecules. The proton shifts are $\sigma^H \sim 0.9$ ppm, $\sigma^H \sim 1.0$ ppm, and $\sigma^H \sim 1.7$ ppm, from cross peaks with 13^1-C=O, 19-C/13^3-C=O, and 17^3-C=O, respectively. To verify this assignment, we have also acquired a 1-D ^{1}H MAS NMR spectrum from a preparation of [95%-^{2}H; 5%-^{1}H] Chl *a* that was aggregated with ^{1}H$_2$O. In these data a broad ^{1}H NMR response centered around 1.4 ppm is observed from the four protons from the water molecules, which corroborates our assignment of the correlation signals with the carbonyls to the protons of structural water molecules.

It is easy to accommodate the water in the model of the structure, since a water bridge is already found in the ethyl-chlorophyllide *a* homologue. In Fig. 5, a gap is left open between the Mg and the carbonyl functionalities of the surrounding Chl *a* moieties. Incorporation of two water molecules in the gap can thus stabilize the Chl *a* aggregates by coordination to the Mg and formation of a hydrogen-bonded network to the 13^1, the 13^3, and one of the 17^3 carbonyl oxygens of the surrounding Chl *a* (*24*). Such a hydrogen-bonding network is accomplished most effectively if the 13^1-C=O of a second molecule is at the same side of the Chl *a* ring as the 13^3-C=O of a first molecule. In this way the stabilization of the aggregate with two structural water molecules favors a single sliding direction for the stacks. In addition, the opposite sliding direction is energetically unfavorable due to steric hindrance of the 13^2 side chain with a neighboring Chl *a* in the stack (*6, 25*).

Finally, we have briefly investigated the possibility of having the Mg coordinated by an OH⁻, which could in principle occur if two or more water molecules would redistribute their protons and the OH⁻ would be compensated by an H_3O^+ in the network. The MNDO-d calculations predict that for an OH⁻ ligand large shifts relative to the neutral form should arise for the 3 side chain. The calculated charge variations alternate in sign along the side chain and would be accompanied by $\Delta\sigma^C$ up to ~5 ppm, of the 5-, 8-, 12-, and 15-C. This is clearly excluded by the experimental data and an OH⁻ coordination is unlikely.

A global model for the static suprastructure can be proposed from MAS NMR by making use of the additional spectroscopic information this technique provides: small linewidths, relaxation times that are essentially the same over the entire molecule, and the absence of conformational shifts. In the Chl a aggregates the mobility is highly restricted. For the Chl a ring system, the ¹³C linewidths of 120–200 Hz, the well-defined pattern of carbon and proton aggregation shifts relative to Chl a in solution, and the observation of homonuclear and heteronuclear distance constraints all provide converging evidence that the rings are forming a highly ordered, microcrystalline environment. In the ¹H–¹³C dataset in Fig. 4 the correlations involving only ring carbons or the P1-CH₂ and P2-CH moieties are elongated parallel to the ¹H axis, while the intramolecular correlations with carbons of the saturated part of the phytyl chain, P4–P15, appear slightly tilted. The tilting is attributed to correlated ¹H

and ¹³C dispersion due to small inhomogeneous broadening, by ~1.5 ppm. In addition, in the ¹³C homonuclear correlation spectrum in Fig. 2, most of the correlations associated with the phytyl chain are similarly broadened. In particular the correlations involving P3 and P4 are broad at the base and extend over 2–3 ppm. The small but systematic inhomogeneous broadening of the signals from phytyl carbons provides evidence for a minor conformational heterogeneity of the saturated part of the chains, which contrasts with the highly ordered structure of the rings. It shows that the domains comprising the Chl a rings and sections with phytyl chains are spatially separate regions in the aggregate. It can be emphasized, however, that the tails are homogeneously ordered, albeit not near to crystallinity as the rings, and that the heterogeneity for the tails is very modest, in contrast to, for instance, the heterogeneity commonly observed for polymers and plastics. In addition there is no evidence for conformational shifts for the tails, which should therefore be stretched.

Chl a/H₂O can form bilayers by aligning two sheets back to back (Fig. 6A), while a tight 3-D suprastructure can be established by arranging multiple bilayers to form a laminar structure with aligned and interdigitating phytyl chains (Fig. 6B). The Chl a rings in the layers are arranged in a 2-D hexagonal lattice, and there is sufficient space between the phytyl chains to accommodate the chains of an adjacent bilayer. Such an arrangement is strongly corroborated by the recent detection of long-range
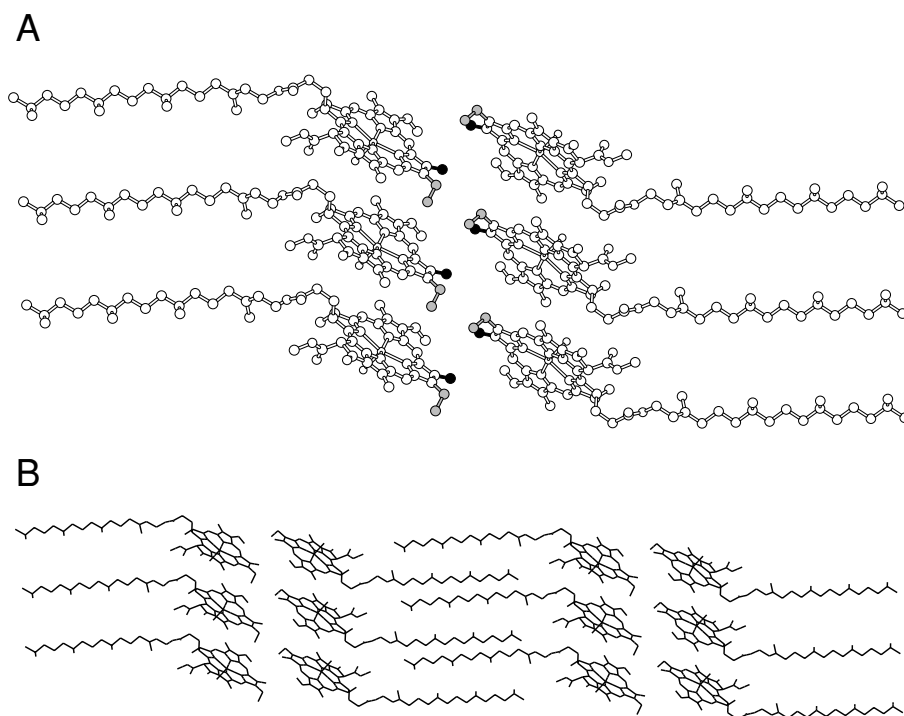
FIG. 6. Schematic representation of a bilayer formed from two sheets of aggregated Chl a/H₂O (A) and of a laminar arrangement of bilayers (B). The orientation of the 2-D sheets is perpendicular to the plane of the paper and the view is parallel to the stack. The 7-Me and 8-Et moieties in (A) are shown in black and gray, respectively.

intermolecular correlations between different parts of the phytyl chains (*26*). In the model for the structure according to Fig. 6, highly ordered rings are spatially separated from aligned and somewhat disordered phytyl regions, in agreement with our data. The alternative of stacking sheets back to front would inevitably give rise to random folding or dynamics of the tails to fill up the open space. This is unlikely, since this would give rise to differences in relaxation times, conformational ^{13}C shifts, or pronounced inhomogeneous line broadening, which are *not* observed. The relatively broad lines from the P3 and P4 may reflect additional strain associated with a twist of the phytyl chains out of plane, perpendicular to the bilayer region formed by the rings.

From the MNDO-*d* calculations we estimate an electric dipole moment of 6.2 D for a chlorophyllide monomer with a water molecule ligated to the Mg. The direction of this dipole moment is from ring III to ring I and $\sim$30° out of the plane of the macroaromatic cycle toward the H_2O ligand. In the self-assembled stack in the NMR model of Fig. 5, such dipoles line up approximately, and in the sheet the dipole moments associated with individual stacks are also oriented in a parallel fashion. In the bilayer, the resultant electric dipoles associated with opposite sheets are oriented partially antiparallel. This arrangement may contribute to the stabilization of a bilayer structure, since the electrostatic forces between resultant dipole moments may form an important contribution to driving the self-assembly process on larger length scales. In contrast, in the dimer form that is found in solution, the dipoles would be largely compensated within the dimer due to an antiparallel orientation (*21, 22*).

The 3-D model in Fig. 6B is a triclinic laminar arrangement with space group *p*1. It has two Chl *a* molecules per unit cell and cell parameters $a = c = \sim$8.9 Å and $\beta = 120.0°$. This model is again consistent with the previously reported data for the relevant homologues (*27, 28*). First, electron microscopy has revealed that Chl *a* is capable of forming a layered structure of at least 10 plates in the dimension perpendicular to the sheets (*29*). The 3-D model in Fig. 6B is also consistent with low-resolution X-ray data obtained for a semiordered preparation of Chl *a* that provides additional evidence that the two Chl *a* molecules in the unit cell are not symmetry related. In particular the possibility of a $p3_1$ symmetry due to back to front stacking of the sheets, as in the crystals of ethyl-chlorophyllide *a*, would be inconsistent with the low-resolution diffraction data (*24, 27–29*).

The narrow NMR lines reveal a very densely packed structure, and the tightest fit on the interface of the model in Fig. 6 can be achieved by rotation of the 8-ethyl moieties in one layer around the 8–8^1 bonds. These are the only structurally relevant conformational degrees of freedom that are allowed by the shift constraints. In this way the doubling of the signals observed in MAS NMR can be accommodated. The 8^2 of one layer can be rotated into cavities between the rings forming the sheet. In this arrangement the 7-methyl are sticking out and can be accommodated by the cavities of an opposite layer in which both

the 7-methyl and the 8-ethyl are pointing outward. In this way two sheets can form a bilayer. The conformational symmetry breaking due to a rotation of the 8-ethyl raises the question of whether this small systematic perturbation at the molecular level can affect the suprastructure of the aggregate on a much larger length scale. For instance, to form a micellar arrangement without solvent, a bilayer tube can be proposed. It was observed with electron microscopy that single bilayer plates of microcrystalline Chl *a*/H_2O have a tendency to curl, with a radius of $\sim$500 Å (*29*).

However, the small linewidth of 0.8–1.3 ppm of the ^{13}C NMR response imposes a strong restraint with respect to the minimal radius a curved bilayer can have in a polycrystalline sample. For a curved bilayer the two sheets will have an opposite bending. The spacing between the Chl *a* rings in Fig. 5 is about 3.7 Å, and differences in overlap regions between the Chl *a* in opposite sheets constituting the tubular structure should be small, since the variation of the chemical shift due to ring-current effects between the Chl *a* in the bilayer is less than $\sim$0.1 ppm, the accuracy of the ^{13}C assignment. At least 60 stacks in both layers are required to have highly similar overlap regions in the two layers, within 1 Å, which is necessary for a linewidth of $\sim$1 ppm. This leads to a lower limit of $\sim$100 Å for a bend radius. A smaller radius would inevitably give rise to a doubling of many signals.

The dipolar correlation methods can only provide spatial information at the microscopic level, while the structure of a space-filled solid has to be self-consistent at all relevant length scales. This provides additional constraints on the microscopic structure. Probably the only way at present to circumvent the problem of propagation of errors is to adhere to a homology modeling approach presented above, where a model involves a classification of possible arrangements that have been observed at various length scales, for oligomers, self-assembled mesoscopic structures, and (semi-)crystals of analogues or related species. The model for the structure obtained in this way is thus partly based on consistency checks against complementary information obtained for related systems. Thus, we cannot claim that the model in Fig. 6 is unique. On the other hand, according to MAS NMR we converge upon an arrangement of Chl *a* molecules in sheets. While such sheets can in principle be arranged in various ways or can be curved, we have not yet found another way to organize sheets in a tight fashion to generate the homogeneously ordered space-filled solid that transpires from the high-resolution dipolar correlation spectra than the model presented in Fig. 6.

CONCLUSIONS

In this work we focus on paracrystalline Chl *a*/H_2O. The self-assembled Chl *a* is a paradigm for MAS NMR structure determination in artificial photosynthesis research. It is shown that knowledge about the electronic structure deduced from the solid-state proton assignment, as well as the assignment of several intermolecular heteronuclear (^{1}H–^{13}C) correlations, leads

to a model for the microscopic structure and a proposition for the 3-D organization of the densely packed solid. In this model Chl *a* molecules and H$_2$O line up in 1-D to form stacks and in 2-D to form highly ordered sheets, in a similar way as in crystals of ethyl-chlorophyllide *a*. Part of the proton response is attributed to polarization transfer from protons in water molecules forming a hydrogen-bonding network to the carbonyl moieties in the model. A doubling of some solid-state NMR signals shows that two conformers of Chl *a* are present that are both structurally well defined. It is inferred that pairs of sheets align back to back, mutually rotated over 180°, in a bilayer structure, while a densely packed suprastructure can be established by a laminar stacking of bilayers with interdigitated phytyl chains like in semicrystalline sheets of Chl *a*.

In Fig. 1B the pattern of heteronuclear correlations involving the two methyl groups is summarized. The large circles indicate the range d_{max} for transfer and comprise the intramolecular transfer events. Correlations outside this range are from intermolecular transfer. This picture illustrates that the size of the molecules is important. The shortest intermolecular distances will always be ∼4 Å. It would be difficult to discriminate between intramolecular and intermolecular transfer in, for instance, an amino acid in the solid crystalline state, since regions of intermolecular and intramolecular transfer will overlap. For macromolecules like proteins and for ligands bound to receptors the intramolecular transfer will generally not overlap with intermolecular transfer regions and we anticipate the future use of dipolar correlation spectroscopy for structure and structure–function studies in proteins.

MATERIALS AND METHODS

Highly enriched Chl *a* (>95%^{13}C) was isolated from a cell culture of *Chenopodium rubrum* that was grown from an isotope-enriched medium (*1*). Aggregates of Chl *a* were prepared overnight by hydration in *n*-heptane (*1*). ^{1}H–^{1}H COSY and ^{13}C–^{1}H COSY data for the monomeric Chl *a* in acetone-d_6 solution were obtained with a DMX-600 spectrometer (Bruker, Karlsruhe, Germany). A low concentration ensured that the Chl *a* exists in the monomeric form, in line with previous work (*30, 31*). By using newly obtained and published data, a complete set of ^{1}H and ^{13}C shifts σ_{liq}^H, σ_{liq}^C for a monomer in solution was produced (Table 2). The shifts in solution compare well with literature data reported previously for chlorophylls in various solvents (*23, 30, 31*), and were used for the calculation of aggregation shifts $\Delta\sigma = \sigma - \sigma_{liq}$ (Table 1). The aggregation effects on the chemical shift and the resulting $\Delta\sigma$ are analyzed in terms of classical ring-current calculations which are sufficiently accurate for describing the observed shift differences (*18*). Quantum chemical calculations are not considered to account for the $\Delta\sigma$, since the direct effects of the aggregation on the electronic structure are small.

CP/MAS spectra were recorded at room temperature with a 4-mm double-resonance probe (Bruker, Karlsruhe, Germany). A homebuilt spinning frequency controller was used to keep the spinning speed constant to within a few hertz (*32*). 2-D homonuclear (^{13}C–^{13}C) RFDR dipolar correlation spectra were recorded with simulated phase-sensitive detection in ω_1 (*1, 33*). The protons were decoupled from the carbons by use of the two-pulse phase-modulation (TPPM) decoupling scheme during ^{13}C acquisition in every experiment and during ^{13}C evolution and mixing in the homonuclear (^{13}C–^{13}C) correlation experiments (*34*). Pulses of 8 μs with a phase-modulation angle of 20° were used for the TPPM decoupling with a ^{1}H RF power corresponding with 60 kHz nutation frequency. The correlation spectra were recorded with a ^{13}C ramp to broaden the CP matching profile at high MAS rates (*35*).

To suppress the homonuclear ^{1}H interactions in the 2-D heteronuclear (^{1}H–^{13}C) dipolar correlation spectroscopy, FSLG irradiation was employed during the proton evolution (Fig. 3) (*4, 36*). In addition, Lee–Goldburg cross-polarization (LG-CP) was used for selective heteronuclear polarization transfer (*8, 37*). Both ^{13}C and ^{1}H solid-state shifts are referenced to TMS. The solid ^{1}H shifts are calibrated by matching the ^{1}H response of the phytyl tails in the aggregate with the corresponding resonances of the monomer in solution. The scaling factor for the ^{1}H chemical shifts in the FSLG experiments was determined experimentally for the Chl *a* by plotting the FSLG proton response against the corresponding nonscaled proton shifts (*5, 9*).

Semiempirical quantum chemical calculations were performed using the MOPAC 97 code incorporated in the Chemoffice package (Cambridgesoft, Cambridge, MA) (*38*). An ethyl-chlorophyllide *a* monomer with H$_2$O, THF, or OH$^-$ as the fifth ligand to the Mg was modeled with MNDO-*d* parametrization (*39, 40*). The ethyl-chlorophyllide *a* with the Mg coordinated with a single water molecule was taken from the X-ray structure and was used as a starting point. It was verified that MNDO-*d* optimization by energy minimization reproduces the monomer ring structure observed experimentally by X-ray (*24*). After a full optimization run, the water was deprotonated or replaced by a THF molecule, followed again by a full optimization of the structure. Estimates of atomic charge densities were evaluated with the Mulliken population analysis on the optimized structures (*41*).

REFERENCES

1. G. J. Boender, J. Raap, S. Prytulla, H. Oschkinat, and H. J. M. de Groot, MAS NMR structure refinement of uniformly ^{13}C enriched chlorophyll *a*/water aggregates with 2D dipolar correlation spectroscopy, *Chem. Phys. Lett.* **237,** 502–508 (1995).

2. S. P. Brown, I. Schnell, J. D. Brand, K. Müllen, and H. W. Spiess, An investigation of π–π packing in a columnar hexabenzocoronene by fast magic-angle spinning and double-quantum ^{1}H solid-state NMR spectroscopy, *J. Am. Chem. Soc.* **121,** 6712–6718 (1999).

3. B.-J. van Rossum, G. J. Boender, F. M. Mulder, J. Raap, T. S. Balaban, A. Holzwarth, K. Schaffner, S. Prytulla, H. Oschkinat, and H. J. M. de Groot, Multidimensional CP-MAS ^{13}C NMR of uniformly enriched chlorophyll, *Spectrochim. Acta A* **54,** 1167–1176 (1998).

4. B.-J. van Rossum, H. Förster, and H. J. M. de Groot, High-field and high-speed CP-MAS ^{13}C NMR heteronuclear dipolar-correlation spectroscopy of solids with frequency-switched Lee-Goldburg homonuclear decoupling, *J. Magn. Reson.* **124,** 516–519 (1997).

5. B.-J. van Rossum, C. P. de Groot, V. Ladizhansky, S. Vega, and H. J. M. de Groot, A method for measuring heteronuclear (^{1}H–^{13}C) distances in high-speed MAS NMR, *J. Am. Chem. Soc.* **122,** 3465–3472 (2000).

6. D. L. Worcester, T. J. Michalski, and J. J. Katz, Small-angle neutron scattering studies of chlorophyll micelles: Models for bacterial antenna chlorophyll, *Proc. Natl. Acad. Sci. USA* **83,** 3791–3795 (1986).

7. T. S. Balaban, A. R. Holzwarth, K. Schaffner, G. J. Boender, and H. J. M. de Groot, CP-MAS ^{13}C dipolar correlation spectroscopy of ^{13}C enriched chlorosomes and isolated bacteriochlorophyll c aggregates of *Chlorobium tepidum*: The self-organization of pigments is the main structural feature of chlorosomes, *Biochemistry* **34,** 15259–15266 (1995).

8. B.-J. van Rossum, S. Prytulla, H. Oschkinat, and H. J. M. de Groot, Biological MAS NMR in high magnetic fields, *in* "Magnetic Resonance and Related Phenomena" (D. Ziessow, W. Lubitz, and F. Lendzian, Eds.), Vol. 1, pp. 38–39, Technische Universität, Berlin (1998).

9. B.-J. van Rossum, G. J. Boender, and H. J. M. de Groot, High magnetic field for enhanced proton resolution in high-speed CP/MAS heteronuclear ^{1}H–^{13}C dipolar-correlation spectroscopy, *J. Magn. Reson. A* **120,** 274–277 (1996).

10. R. G. Griffin, Dipolar recoupling in MAS spectra of biological solids, *Nat. Struct. Biol. NMR Suppl.* **7,** 508–512 (1998).

11. J. M. Griffiths, K. V. Lakshmi, A. E. Bennett, J. Raap, C. M. van der Wielen, J. Lugtenburg, J. Herzfeld, and R. G. Griffin, Dipolar correlation NMR spectroscopy of a membrane protein, *J. Am. Chem. Soc.* **116,** 10178–10181 (1994).

12. P. J. E. Verdegem, P. H. M. Bovee-Geurts, W. J. de Grip, J. Lugtenburg, and H. J. M. de Groot, Retinylidene ligand structure in bovine rhodopsin, metarhodopsin-I and 10-methylrhodopsine from internuclear distance measurements using ^{13}C-labeling and 1-D rotational resonance MAS NMR, *Biochemistry* **38,** 11316–11324 (1999).

13. R. R. Ketcham, W. Hu, and T. A. Cross, High-resolution conformation of gramicidin-A in a lipid bilayer by solid-state NMR, *Science* **261,** 1457–1460 (1993).

14. H. Spiesecke and W. G. Schneider, The determination of π-electron densities in Azulene from C^{13} and H^1 nuclear resonance shifts, *Tetrahedron Lett.* **14,** 468–472 (1961).

15. R. J. Weesie, F. J. H. M. Jansen, J. C. Merlin, J. Lugtenburg, G. Britton, and H. J. M. de Groot, ^{13}C Magic angle spinning NMR analysis and quantum chemical modeling of the bathochromic shift of astaxanthin in α-crustacyanin, the blue carotenoprotein complex in the carapace of the lobster *Homarus gammarus, Biochemistry* **36,** 7288–7296 (1997).

16. S. O. Smith, I. Palings, M. E. Miley, J. Courtin, H. J. M. de Groot, J. Lugtenburg, R. A. Mathies, and R. G. Griffin, *Biochemistry* **29,** 8158–8164 (1990).

17. It should be mentioned here that the correlation terms were not included in these calculations.

18. C. Giessner-Prettre and B. Pullman, Intermolecular nuclear shielding due to aromatic amino acids of proteins and porphyrins, *J. Theor. Biol.* **31,** 287–294 (1971).

19. D. S. Boudreaux, R. R. Chance, J. L. Brédas, and R. Silbey, Solitons and polarons in polyacetylene: Self-consistent-field calculations of the effect of neutral and charged defects on molecular geometry, *Phys. Rev. B* **28,** 6927–6936(1983).

20. J. J. Katz, M. K. Bowman, T. J. Michalski, and D. L. Worcester, Chlorophyll aggregation: Chlorophyll/water micelles as models for *in vivo* long-wavelength chlorophyll, *in* "Chlorophylls" (H. Scheer, Ed.), pp. 211–235, CRC Press, Boca Raton, FL (1991).

21. R. J. Abraham, D. A. Goff, and K. M. Smith, NMR spectra of porphyrins. Part 35. An examination of the proposed models of the chlorophyll *a* dimer, *J. Chem. Soc. Perkin Trans.* **1,** 2443–2451 (1988).

22. R. J. Abraham and K. M. Smith, NMR spectra of porphyrins. 21. Application of the ring-current model to porphyrin and chlorophyll aggregation, *J. Am. Chem. Soc.* **105,** 5734–5741 (1983).

23. R. J. Abraham and A. E. Rowan, Nuclear magnetic resonance spectroscopy of chlorophyll, *in* "Chlorophylls" (H. Scheer, Ed.), pp. 797–834, CRC Press, Boca Raton, FL (1991).

24. H. C. Chow, R. Serlin, and C. E. Strouse, The crystal and molecular structure and absolute configuration of ethyl chlorophyllide *a* dihydrate. A model for the different spectral forms of chlorophyll *a*, *J. Am. Chem. Soc.* **97,** 7230–7237 (1975).

25. T. Oba, T. Watanabe, M. Mimuro, M. Kobayashi, and S. Yoshida, Aggregation of chlorophyll *a'* in aqueous methanol, *Photochem. Photobiol.* **63,** 639–648 (1996).

26. I. de Boer, L. Bosman, J. Raap, H. Oschkinat, and H. J. M. de Groot, submitted (2001).

27. G. Donnay, Crystal data on chlorophyll *a*, *Arch. Biochem. Biophys.* **80,** 80–85 (1959).

28. C. Kratky and J. D. Dunitz, Ordered aggregation states of chlorophyll *a* and some derivatives, *J. Mol. Biol.* **113,** 431–442 (1977).

29. E. E. Jacobs, A. E. Vatter, and A. S. Holt, Crystalline chlorophyll and bacteriochlorophyll, *Arch. Biochem. Biophys.* **53,** 228–238 (1954).

30. S. Lötjönen and P. H. Hynninen, ^{13}C nmr spectra of chlorophyll *a*, chlorophyll *a'*, pyrochlorophyll *a* and the corresponding pheophytins, *Org. Magn. Reson.* **21,** 757 (1983).

31. P. H. Hynninen and S. Lötjönen, Steric interactions between the peripheral substituents of 10(*S*)-chlorophyll derivatives and its conformational consequences, a proton magnetic resonance study, *Magn. Reson. Chem.* **23,** 605–615 (1985).

32. H. J. M. de Groot, V. Copié, S. O. Smith, P. J. Allen, C. Winkel, J. Lugtenburg, J. Herzfeld, and R. G. Griffin, Magic-angle-sample-spinning NMR difference spectroscopy, *J. Magn. Reson.* **77,** 251–257 (1988).

33. A. E. Bennett, J. H. Ok, R. G. Griffin, and S. Vega, Chemical shift correlation spectroscopy in rotating solids: Radio frequency-driven dipolar recoupling and longitudinal exchange, *J. Chem. Phys.* **96,** 8624–8627 (1992).

34. A. E. Bennett, C. M. Rienstra, M. Auger, K. V. Lakshmi, and R. G. Griffin, Heteronuclear decoupling in rotating solids, *J. Chem. Phys.* **103,** 6951–6958 (1995).

35. G. Metz, X. Wu, and S. O. Smith, Ramped-amplitude cross polarization in magic-angle-spinning NMR, *J. Magn. Reson. A* **110,** 219–227 (1994).

36. A. Bielecki, A. C. Kolbert, and M. H. Levitt, Frequency-switched pulse sequences: Homonuclear decoupling and dilute spin NMR in solids, *Chem. Phys. Lett.* **155,** 341–346 (1989).

37. P. Caravatti, G. Bodenhausen, and R. R. Ernst, Heteronuclear solid-state correlation spectroscopy, *Chem. Phys. Lett.* **89,** 363–367 (1982).

38. J. J. P. Stewart, Mopac: A semiempirical molecular orbital program, *J. Comput-Aided Mol. Design* **4,** 1–105 (1990).

39. M. J. S. Dewar and W. Thiel, Ground states of molecules. 38. 1. The MNDO Method. Approximation and parameters, *J. Am. Chem. Soc.* **99,** 4899–4917 (1977).

40. W. Thiel and A. A. Voityuk, Extension of MNDO to d orbitals: Parameters and results for the second-row elements and for the zinc group, *J. Phys. Chem.* **100,** 616–626 (1996).

41. R. S. Mulliken, Electronic population analysis on LCAO-MO molecular wave functions, *J. Chem. Phys.* **23,** 1833–1840 (1955).